Theory for the anomalous electron transport in Hall effect thrusters. II. Kinetic model

T. Lafleur,[1,2,a)] S. D. Baalrud,[3] and P. Chabert[1]
[1]*Laboratoire de Physique des Plasmas, CNRS, Sorbonne Universités, UPMC Univ Paris 06, Univ Paris-Sud, Ecole Polytechnique, 91128 Palaiseau, France*
[2]*Centre National d'Etudes Spatiales (CNES), F-31401 Toulouse, France*
[3]*Department of Physics and Astronomy, University of Iowa, Iowa City, Iowa 52242, USA*

(Received 4 February 2016; accepted 19 April 2016; published online 9 May 2016)

In Paper I [T. Lafleur *et al.*, Phys. Plasmas **23**, 053502 (2016)], we demonstrated (using particle-in-cell simulations) the definite correlation between an anomalously high cross-field electron transport in Hall effect thrusters (HETs), and the presence of azimuthal electrostatic instabilities leading to enhanced electron scattering. Here, we present a kinetic theory that predicts the enhanced scattering rate and provides an electron cross-field mobility that is in good agreement with experiment. The large azimuthal electron drift velocity in HETs drives a strong instability that quickly saturates due to a combination of ion-wave trapping and wave-convection, leading to an enhanced mobility many orders of magnitude larger than that expected from classical diffusion theory. In addition to the magnetic field strength, B_0, this enhanced mobility is a strong function of the plasma properties (such as the plasma density) and therefore does not, in general, follow simple $1/B_0^2$ or $1/B_0$ scaling laws. *Published by AIP Publishing*. [http://dx.doi.org/10.1063/1.4948496]

I. INTRODUCTION

Despite being a mature technology that has seen almost 60 years of development, there are a number of aspects of Hall effect thruster (HET) operation that are still not understood, resulting in the continued need for semi-empirical approaches to their design.[1–3] Of these unresolved issues, a recent roadmap article[4] identified the poor understanding of the anomalously high electron transport across the thruster magnetic field as one of the main hurdles to future development and highlighted the need for self-consistent models of this phenomenon in order to make further progress. Because HETs are often used in station-keeping or long-term scientific missions, they are required to operate for many thousands of hours. However, bombardment of plasma-facing surfaces inside the thruster, such as the dielectric walls, results in erosion[3,5] which can degrade the thruster performance or eventually cause complete failure.[3] Therefore, qualification of newly designed thrusters is an important process, but one which typically requires many months or years of continual testing in high-vacuum space simulation chambers. This testing is expensive and time-consuming, and highlights the need for accurate models and simulations to help predict erosion rates and lifetimes without needing such long-term experimental work. In addition, these models are needed to help design and develop new thrusters to meet future performance requirements, while minimizing costly experimental optimization campaigns.

Over the last few decades, a large number of different multi-dimensional simulations have been developed to help predict HET operation. These include simulations where both ions and electrons are treated using a fluid description,[6–8] hybrid simulations using fluid electrons and a kinetic description for ions,[9–11] and fully kinetic particle-in-cell (PIC) simulations.[12–15] Traditionally, many of these models have simulated only the axial[9] or the axial-radial dimensions,[12] because of the apparent azimuthal symmetry exhibited by the thruster. However, in each of these simulations, including the axial-radial PIC simulations,[12] an enhanced electron collisionality was needed in order to obtain results similar to experiments.[8–10,16–22] This anomalous collisionality is usually chosen empirically based on phenomenological arguments and experimental measurements, and no self-consistent model exists yet for its description. This reliance on experiment significantly reduces the predictive power and utility of present simulations.

Although HETs appear mechanically symmetric in the azimuthal direction, the radial applied magnetic field, together with the axial electric field, produces a preferred electron $\mathbf{E} \times \mathbf{B}$ drift that breaks this symmetry. Consequently, experimental measurements,[23–28] as well as simulations modelling the azimuthal direction (such as in 2D axial-azimuthal,[13] 2D radial-azimuthal,[14,29] or simply 1D azimuthal simulations[30–32]), have shown the presence of an instability with fluctuations in the azimuthal electric field and the electron density. These fluctuations typically have frequencies in the MHz range, and wavelengths of the order of mm's.[13,14,16] In addition, the magnitude of the azimuthal electric field fluctuations can be similar to that of the axial electric field itself. Perhaps the most convincing demonstration of the importance of these azimuthal instabilities on HET operation was presented in the 2D PIC simulations of Ref. 13. There the axial-azimuthal directions of the thruster were simulated, and with no free parameter or empirical collisionality required, the simulations reproduced a number of experimental observations. Although these simulations did not model the radial direction, an approximate model for

a)Electronic mail: trevor.lafleur@lpp.polytechnique.fr

electron-wall collisions was included. Electron-wall collisions were not sufficient to explain the observed electron transport, and since the radial wall sheaths, as well as secondary electron emission, were not present, the simulations suggest that these effects are not the dominant mechanisms responsible for the anomalous transport.

While the axial-azimuthal simulations of Ref. 13 provide important insight into the anomalous electron transport mechanism, they ignore the radial direction which is vital for the accurate modelling of real-life HET performance and lifetimes. Since simulations of the axial-radial directions alone do not observe this anomalous transport, it appears that fully kinetic 3D PIC simulations are in principle needed. However, because of numerical simulation stability criteria, such simulations require massive parallelization and are inherently complex and time consuming to run, making it difficult to utilize them in thruster design. In contrast, electron-fluid based simulations are significantly faster to run, and could be easily used to evaluate new designs, and while these models do not self-consistently account for the anomalous transport,[10,16,17] good agreement can be obtained by introducing anomalous electron collisionalities based on experiment.[6,16,21,33,34] Thus if an externally developed theory of this anomalous transport can be found,[19,35] the reliance on experiment could be reduced and a self-consistent method for simulating HETs, and an increased physical understanding, obtained.

In Paper I,[31] we presented a simple 1D PIC simulation similar to that discussed in Ref. 30 that modelled the azimuthal direction of a Hall effect thruster. This simulation included a mutually perpendicular axial electric field, $\mathbf{E}_0$, and radial magnetic field, $\mathbf{B}_0$, with the $\mathbf{E}_0 \times \mathbf{B}_0$ direction in the azimuthal direction. By controlling the plasma density in the simulation, we showed that at very low densities, the cross-field electron transport was classical, but that as the plasma density increases, a strong instability develops in the azimuthal direction, and the cross-field transport becomes significantly enhanced. Associated with this instability are fluctuations in both the azimuthal electric field, δE_θ, as well as the electron density, δn_e, which results in a non-vanishing spatially and temporally averaged (over the characteristic instability wavelength and period) force: $q\langle \delta n_e \delta E_\theta \rangle$. We then presented a theory where the effective cross-field electron mobility is given by

$$\mu_{eff} = \frac{\frac{q}{m\nu_m}}{1+\frac{\omega_{ce}^2}{\nu_m^2}}\left[1-\frac{\omega_{ce}}{\nu_m}\frac{\langle \delta n_e \delta E_\theta \rangle}{n_e E_0}\right], \tag{1}$$

where q and m are the electron charge and mass, respectively, ν_m is the electron-neutral momentum transfer collision frequency, and $\omega_{ce} = qB_0/m$ is the electron cyclotron frequency. By explicitly evaluating the correlation term, $\langle \delta n_e \delta E_\theta \rangle$, from the PIC simulations, we demonstrated that the enhanced electron transport could be completely described by Eq. (1). In the present work, we develop a kinetic theory to explicitly calculate this correlation term and obtain an analytical solution for the anomalous mobility/collisionality that aids physical understanding and offers an approximate formula that could be incorporated into fluid-based simulations to self-consistently model HETs.

II. KINETIC MODEL

A. Plasma kinetic equations

We take as our starting point the Vlasov equation and assume that the particle distribution function for a species s can be separated into an equilibrium component, f_s, and a fluctuating component, δf_s (and similarly for the electric and magnetic fields). This allows the derivation of the standard plasma kinetic equations for each component[36,37]

$$\frac{\partial f_s}{\partial t} + \mathbf{v}\cdot\frac{\partial f_s}{\partial \mathbf{x}} + \frac{q_s}{m_s}(\mathbf{E}+\mathbf{v}\times\mathbf{B})\cdot\frac{\partial f_s}{\partial \mathbf{v}} = -\frac{q_s}{m_s}\left\langle (\delta\mathbf{E}+\mathbf{v}\times\delta\mathbf{B})\cdot\frac{\partial \delta f_s}{\partial \mathbf{v}}\right\rangle, \tag{2}$$

$$\frac{\partial \delta f_s}{\partial t} + \mathbf{v}\cdot\frac{\partial \delta f_s}{\partial \mathbf{x}} + \frac{q_s}{m_s}(\mathbf{E}+\mathbf{v}\times\mathbf{B})\cdot\frac{\partial \delta f_s}{\partial \mathbf{v}} = -\frac{q_s}{m_s}(\delta\mathbf{E}+\mathbf{v}\times\delta\mathbf{B})\cdot\frac{\partial f_s}{\partial \mathbf{v}} + \frac{q_s}{m_s}\left[\left\langle (\delta\mathbf{E}+\mathbf{v}\times\delta\mathbf{B})\cdot\frac{\partial \delta f_s}{\partial \mathbf{v}}\right\rangle - (\delta\mathbf{E}+\mathbf{v}\times\delta\mathbf{B})\cdot\frac{\partial \delta f_s}{\partial \mathbf{v}}\right], \tag{3}$$

where $\mathbf{x}$ and $\mathbf{v}$ are phase space coordinates, t is time, q_s and m_s are the charge and mass of species s, $\mathbf{E}(\mathbf{x}, t)$ and $\mathbf{B}(\mathbf{x}, t)$ are equilibrium electric and magnetic field components, and $\delta\mathbf{E}(\mathbf{x}, t)$ and $\delta\mathbf{B}(\mathbf{x}, t)$ are fluctuating electric and magnetic field components. Since the objective is to model transport associated with the electrostatic instability observed in previous PIC simulations,[12–15,30,31] we will ignore any fluctuations in the magnetic field and set $\delta\mathbf{B} = 0$. Then the right-hand side of Eq. (2) represents a collision operator describing collisions between charged particles.[37,38] Here, we will assume that the only species are electrons and singly charged ions. By multiplying Eq. (2) by $m_s\mathbf{v}$ and integrating over all velocities, the electron momentum conservation equation is obtained

$$\frac{\partial}{\partial t}(mn_e\mathbf{v}_{de}) + \nabla\cdot(mn_e\mathbf{v}_{de}\mathbf{v}_{de}) = qn_e(\mathbf{E}+\mathbf{v}_{de}\times\mathbf{B}) - \nabla\cdot\Pi_e + \mathbf{R}_{ei}. \tag{4}$$

Here, q and m are the electron charge and mass, n_e, $\mathbf{v}_{de}$, and Π_e are the electron density, drift velocity, and pressure tensor, and $\mathbf{R}_{ei}$ is an electron-ion frictional drag force (electron-electron collisions conserve momentum between the electron species) given by

$$\mathbf{R}_{ei} = -q\int d^3v\mathbf{v}\frac{\partial}{\partial \mathbf{v}}\cdot\langle \delta\mathbf{E}\delta f_e\rangle = q\int d^3v\langle \delta f_e \delta\mathbf{E}\rangle = q\langle \delta n_e \delta\mathbf{E}\rangle. \tag{5}$$

Here, we have made use of integration by parts, noting that the boundary terms go to zero. Equation (5) demonstrates that electron-ion frictional drag is directly associated with correlations in the fluctuations between the electron density

and the electric field, and connects with the results presented in Paper I.[31] In Sections II B–II F, we explicitly calculate this correlation term. The equations above do not include electron-neutral collisions. We will see below that the neutral gas density in the acceleration and downstream regions of typical HET thrusters is sufficiently low that the effective collision rate due to wave-particle scattering far exceeds that associated with electron-neutral collisions. Hence, electron transport is predominantly anomalous (i.e., associated with wave-particle interactions). The influence of electron-neutral collisions is discussed further in Section II F below.

In what follows we make use of a Cartesian coordinate system to simplify the analysis, where the "axial" thruster dimension is in the z-direction (with unit vector denoted $\hat{\mathbf{k}}$), the "radial" dimension is in the x-direction (with unit vector denoted $\hat{\mathbf{i}}$), and the "azimuthal" dimension is in the y-direction (with unit vector denoted $\hat{\mathbf{j}}$). We also assume that the applied magnetic field, B_x, is only in the x-direction, that there is only an equilibrium electric field, E_z, in the z-direction, and that the ions are unmagnetized.

B. Dispersion relation

Before calculating the electron-ion friction force, we consider the plasma dielectric function and the dispersion relation for electrostatic waves (which will be needed later). A general expression for the plasma dielectric function can be obtained by making use of the method of characteristics[37] and is given by

$$\hat{\varepsilon}(\mathbf{k},\omega) = 1 + \sum_s \frac{q_s^2}{k^2 \epsilon_0 m_s} \int d^3v \frac{\mathbf{k}\cdot \partial f_s/\partial \mathbf{v}}{\bar{\omega}_p}, \tag{6}$$

where

$$\frac{1}{\bar{\omega}_p} = -i \int_0^\infty d\tau \exp[i(\mathbf{k}\cdot\mathbf{d} + \omega\tau)]. \tag{7}$$

Here, $\mathbf{d}$ is a distance obtained from the method of characteristics after integrating over unperturbed particle trajectories (see the Appendix for further details), ϵ_0 is the permittivity of free space, and ω and $\mathbf{k}$ are the fluctuation angular frequency and wavevector. The dispersion relation for a plasma in the presence of a magnetic field has previously been derived in the context of beam cyclotron instabilities in Ref. 39, and more recently, in the context of Hall effect thrusters in Ref. 32. In these works, it was shown that the effect of the magnetic field is to introduce a quantization of the dispersion relation with discrete wave frequency and growth rate bands. Additional work in Ref. 40 however showed that this discrete nature is only significant for very small wavenumbers parallel to the magnetic field (k_x in the notation used here), and that for larger wavenumbers, the dispersion relation simplifies to a modified ion-acoustic type relation. In this case, the only role of the magnetic field is to induce an azimuthal electron drift velocity, $\mathbf{v}_{de} = E_z/B_x\hat{\mathbf{j}}$.

In order to confirm the results above, we have rederived the full dispersion relation associated with Eqs. (6) and (7), which includes finite gyroradius effects, in the Appendix. This result will later be compared with a simplified dispersion relation, which we now derive based on the large gyroradius limit. The Appendix shows that for $\lambda_{De}/\rho \ll 1$ (where $\lambda_{De} = \sqrt{\epsilon_0 T_e/q n_e}$ is the electron Debye length with T_e being the electron temperature in units of eV, and ρ is the electron gyroradius), Eq. (7) simplifies to

$$\frac{1}{\bar{\omega}_p} = \frac{1}{\omega - \mathbf{k}\cdot\mathbf{v}}. \tag{8}$$

We then use a drifting Maxwellian distribution for the ions, and a general drifting distribution for electrons (in anticipation of the friction calculation in Sections II C and II E), given by

$$f_i = \frac{n_i}{\pi^{3/2} v_{Ti}^3} \exp\left[-\frac{(\mathbf{v}-\mathbf{v}_{di})^2}{v_{Ti}^2}\right], \tag{9}$$

$$f_e = \frac{n_e}{v_{Te}^3 \int d^3u' g(\mathbf{u}')} g\left(\frac{\mathbf{v}-\mathbf{v}_{de}}{v_{Te}}\right). \tag{10}$$

Here, n_i is the ion density, $v_{Ti} = \sqrt{2qT_i/M}$ is the ion thermal velocity with T_i and M is the ion temperature and ion mass, $v_{Te} = \sqrt{2qT_e/m}$ is a characteristic electron thermal velocity, and $g(\mathbf{u})$ is a function representing the electron distribution and normalized such that $n_e = \int d^3v f_e$. By then substituting Eqs. (8)–(10) into Eq. (6) and simplifying we obtain

$$\hat{\varepsilon}(\mathbf{k},\omega) = 1 - \frac{\omega_{pi}^2}{k^2 v_{Ti}^2} Z'\left(\frac{\omega - \mathbf{k}\cdot\mathbf{v}_{di}}{k v_{Ti}}\right) + \frac{1}{2k^2\lambda_{De}^2}\int_{-\infty}^{\infty} du_\parallel \frac{dG/du_\parallel}{\zeta - u_\parallel}, \tag{11}$$

where Z is the plasma dispersion function of Fried and Conte,[41] $\omega_{pi} = \sqrt{q^2 n_e/\epsilon_0 M}$ is the ion plasma frequency and we have used quasineutrality so that $n_i \approx n_e$, $G = G(u_\parallel) = \int d^2u g(\mathbf{u}_\perp, u_\parallel)/\int d^3u g(\mathbf{u})$ (with $u_\parallel$ a normalized velocity variable aligned with the wavevector, and $\mathbf{u}_\perp$ perpendicular), and $\zeta = (\omega - \mathbf{k}\cdot\mathbf{v}_{de})/k v_{Te}$. Expanding the plasma dispersion function for large arguments[41] gives $Z'(w) \approx w^{-2} - 2iw\sqrt{\pi}\exp(-w^2)$. As will be shown below, $\omega - \mathbf{k}\cdot\mathbf{v}_{di} \sim k c_s$, where $c_s = \sqrt{qT_e/M}$, and thus $w \propto \sqrt{T_e/T_i}$. Since the electron temperature in typical Hall thrusters can be as high as 25–40 eV,[19,40] we will assume that $T_e/T_i \gg 1$ and neglect the second term in the expansion of the dispersion function. This term is usually associated with ion Landau damping which acts to stabilize an ion-acoustic instability. Since the instability studied here is driven by the electron drift velocity which is of the order of the electron thermal speed rather than the ion-acoustic speed, ion Landau damping is not expected to have a significant effect. Nevertheless, there may be operating conditions where ion Landau damping is important, in which case the present analysis will over-estimate the instability growth rate.

Applying the Plemelj relation to the integral term in Eq. (11) gives

$$\hat{\varepsilon}(\mathbf{k},\omega) = 1 - \frac{\omega_{pi}^2}{(\omega - \mathbf{k}\cdot\mathbf{v}_{di})^2} + \frac{\alpha}{k^2\lambda_{De}^2} - i\frac{\pi\beta}{k^2\lambda_{De}^2}, \tag{12}$$

with

$$\alpha = \frac{1}{2} P \int_{-\infty}^{\infty} du_{\parallel} \frac{dG/du_{\parallel}}{\zeta - u_{\parallel}}, \tag{13}$$

$$\beta = \frac{1}{2} \frac{dG}{du_{\parallel}}\bigg|_{\zeta}, \tag{14}$$

and where P represents the Cauchy principal value. Assuming that the imaginary part in Eq. (12) is small, and using a complex wave frequency (i.e., $\omega = \omega_R + i\gamma$), we can solve for the dispersion relation by setting $\hat{\varepsilon}(\mathbf{k}, \omega) = 0$ to obtain

$$\omega_R \approx \mathbf{k} \cdot \mathbf{v}_{di} \pm \frac{kc_s}{\sqrt{\alpha + k^2 \lambda_{De}^2}}, \tag{15}$$

$$\gamma \approx \pm \frac{\pi \beta k c_s}{2\left(\alpha + k^2 \lambda_{De}^2\right)^{3/2}}. \tag{16}$$

The above equations represent the modified ion-acoustic dispersion relation for a general electron distribution function. If the distribution function is a drifting Maxwellian, $g(\mathbf{u}) = \exp(-\mathbf{u}^2)$, and assuming that $\zeta \approx -\mathbf{k} \cdot \mathbf{v}_{de}/kv_{Te} \ll 1$, then $\alpha \approx 1$, $\beta \approx -\zeta/\sqrt{\pi}$, and hence Equations (15) and (16) simplify to

$$\omega_R \approx \mathbf{k} \cdot \mathbf{v}_{di} \pm \frac{kc_s}{\sqrt{1 + k^2 \lambda_{De}^2}}, \tag{17}$$

$$\gamma \approx \pm \sqrt{\frac{\pi m}{8M}} \frac{\mathbf{k} \cdot \mathbf{v}_{de}}{\left(1 + k^2 \lambda_{De}^2\right)^{3/2}}. \tag{18}$$

Based on this dispersion relation, we note a number of important points: (1) the relation is continuous with wavenumber and the wave frequency is essentially linear in wavenumber for large k_z (since $\mathbf{k} \cdot \mathbf{v}_{di} \approx k_z v_{di}$), (2) there are 2 modes (ω_R^+ and γ^+, and ω_R^- and γ^-), and (3) since $\mathbf{k} \cdot \mathbf{v}_{de} \approx k_y v_{de}$, the growth rate for one mode is positive for $k_y > 0$, while for the second mode it is positive for $k_y < 0$. However, it can be shown that the group velocity, $\partial\omega_R/\partial k_y$, of both modes (as well as the phase velocity, ω_R/k_y) are equal, indicating that the modes are in fact identical.

Having obtained the dispersion relation for a modified ion-acoustic instability with a drifting Maxwellian distribution (the same distribution which is used in the derivation of the full dispersion relation[32]), we now compare this with the full dispersion relation found in the Appendix (Eq. (A4)). Figure 1 shows a comparison for typical HET parameters (representative of the PPS®X000 thruster) where the electron temperature is $T_e = 25\,\text{eV}$, electron density is $n_e = 2 \times 10^{17}\,\text{m}^{-3}$, xenon ion drift velocity is $v_{di} = 1.6 \times 10^4\,\text{ms}^{-1}$, electric field is $E_z = 1 \times 10^4\,\text{Vm}^{-1}$, magnetic field is $B_x = 150\,\text{G}$, and axial wavenumber is $k_z = 0\,\text{m}^{-1}$. These values give an electron azimuthal drift velocity of $v_{de} = E_z/B_x = 6.7 \times 10^5\,\text{ms}^{-1}$, and an ion sound speed of $c_s = 4.3 \times 10^3\,\text{ms}^{-1}$ (hence $v_{de}/c_s \gg 1$). The above parameters are similar to those used in Ref. 40. As can be seen, the ion-acoustic relation is in excellent agreement with the full dispersion relation, except for very small values of $k_x \lambda_{De}$. However, because of the finite channel width in HETs, not all wavelengths, λ, will fit. Since the typical channel width, ΔR, is of the order of 1 cm, the smallest parallel wavenumber that can exist is $k_x^{min} \lambda_{De} \sim 2\pi\lambda_{De}/\Delta R \approx 0.05$. From Fig. 1, we see that for wavenumbers above this, the discrete nature of the full dispersion relation vanishes, and the modified ion-acoustic relation is an excellent approximation. This conclusion is consistent with previous experimental measurements of the dispersion relation,[42,43] where a linear relation is observed instead of a discrete one.

C. Instability-enhanced electron-ion friction force

Developing a theory to predict the correlation term in Eq. (5) is complicated by the fact that nonlinear effects are important in the instability evolution. This can be easily demonstrated as follows. Assuming that the instability is predominantly in the "azimuthal" direction (i.e., $\mathbf{k} \approx k_y \hat{\mathbf{j}}$), we can find the wavenumber giving the maximum growth rate, k_{max}, from $\partial\gamma/\partial k_y = 0$. Using γ from Eq. (16), this gives

$$k_{max} = \pm \frac{1}{\lambda_{De}} \sqrt{\frac{\alpha}{2}} \approx \pm \frac{1}{\sqrt{2}\lambda_{De}}, \tag{19}$$

where we have assumed that $\alpha \approx 1$, which is true for a Maxwellian electron distribution function. Substituting Eq. (19) into Eqs. (17) and (18) gives

$$\omega_{Rmax} = \mathbf{k} \cdot \mathbf{v}_{di} \pm \frac{\omega_{pi}}{\sqrt{3}}, \tag{20}$$

$$\gamma_{max} = \sqrt{\frac{\pi m}{54M}} \frac{v_{de}}{\lambda_{De}}. \tag{21}$$

The growth time of the instability electric field energy density is therefore $\tau_g = 1/(2\gamma_{max})$. For the numerical parameters given in Section II B, this gives $\tau_g \sim 0.1\,\mu\text{s}$. The group velocity of the instability is given by

$$\mathbf{v}_g = \frac{\partial\omega_R}{\partial\mathbf{k}} = \mathbf{v}_{di} \pm \frac{\mathbf{k}}{k} \frac{c_s}{\left(1 + k^2 \lambda_{De}^2\right)^{3/2}} \approx \mathbf{v}_{di}. \tag{22}$$

Thus the "convection time" out of the thruster acceleration region is $\tau_c \approx L_{acc}/v_{di}$, where L_{acc} is the length of the acceleration region of the thruster. Using $L_{acc} \sim 1\,\text{cm}$, we find $\tau_c \approx 0.6\,\mu\text{s}$. Thus $\tau_c/\tau_g \gg 1$, and hence the instability will have a very long time to grow before being convected away. Therefore, nonlinear effects are needed to model the electron-ion friction force. These nonlinear effects will determine both the amplitude of the instability, as well as the growth rate at saturation. In performing the estimates above, we have neglected the effect of neutral collisions which would act to reduce the instability growth rate. The neutral density in the thruster acceleration and downstream regions is typically between 10^{17} and $10^{18}\,\text{m}^{-3}$.[16] Using a representative momentum transfer rate factor of $2.5 \times 10^{-13}\,\text{m}^{-3}\,\text{s}^{-1}$,[9] we find an electron-neutral collisional mean free time of around 4–40 μs. Since this is much higher than both the instability growth time and the convection time of the wave

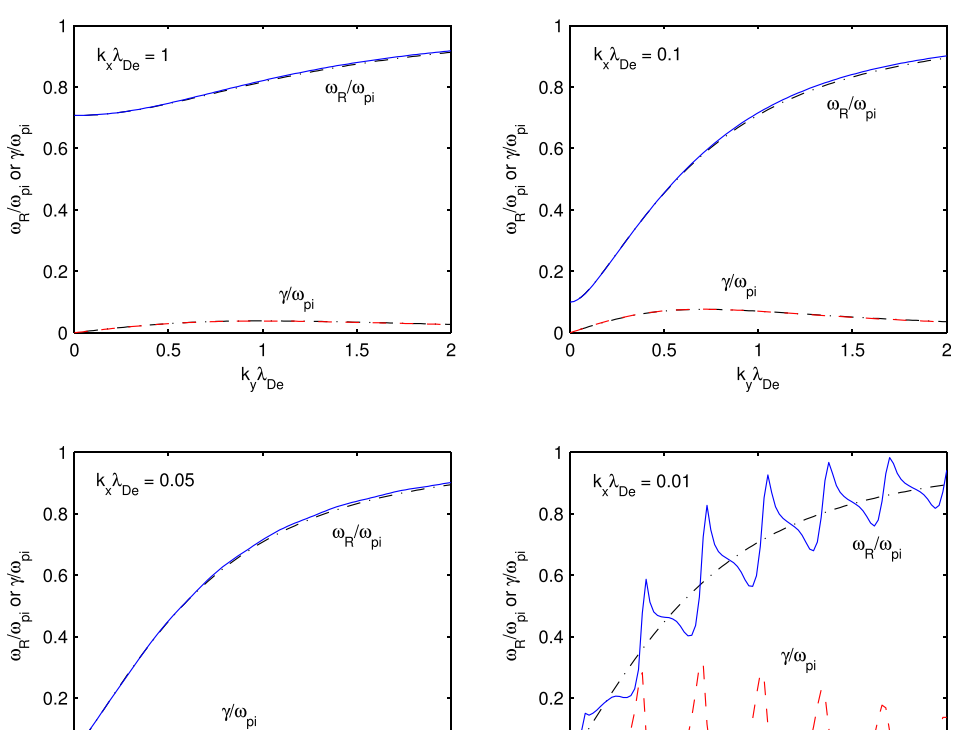

FIG. 1. Comparison of the wave angular frequency (ω_R/ω_{pi}) and growth rate (γ/ω_{pi}) for the modified ion-acoustic dispersion relation (dashed-dotted lines), and the full dispersion relation (solid lines for ω_R/ω_{pi} and dashed lines for γ/ω_{pi}), for different values of the parallel wavenumber, $k_x\lambda_{De}$. For typical HETs, the minimum wavenumber that satisfies the radial boundary conditions is $k_x\lambda_{De} \sim 0.05$.

in the axial direction, collisions are expected to play a negligible role in the instability evolution.

Since the group velocity of the instability is finite (see Eq. (22)), the growth rate at saturation will not, in general, be zero. Rather, velocity-space diffusion of the electron distribution function will occur so as to significantly reduce the initial growth rate[44] leading to a value at steady-state that is balanced by wave-convection; that is $\tau_g^{sat} \sim \tau_c$. Before obtaining these saturation parameters, we now calculate a general expression for the electron-ion friction force.

Based on the PIC simulations in Paper I,[31] ion-wave trapping was observed which suggests that the instability is dominated by a single mode (which occurs at the maximum growth rate). This is also consistent with previous experimental[42] and 2D PIC simulation results.[16] Thus we will assume an instability with a single frequency and wavenumber (which is predominantly in the "azimuthal" direction), which at equilibrium has: $\delta E_y = \mathrm{Re}\{\delta\tilde{E}e^{i(k_y y-\omega_R t)}\}$ and $\delta f_e = \mathrm{Re}\{\delta\tilde{f}_e e^{i(k_y y-\omega_R t)}\}$. Here, $\delta\tilde{E}$ and $\delta\tilde{f}_e$ are the complex fluctuation electric field and electron distribution function amplitudes at saturation, respectively. The distribution function can be written in terms of the electric field by making use of Eq. (3)

$$\delta\tilde{f}_e = \frac{|q|\delta\tilde{E}}{m}\frac{i}{\omega - k_y v_y}\frac{\partial f_e}{\partial v_y}. \tag{23}$$

Here, we have ignored the electric and magnetic field terms on the left-hand side of Eq. (3) (justified based on the comparison in Section II B), and the nonlinear terms on the right-hand side (which will be justified *a posteriori* below). The electron density is given by $\delta n_e = \int d^3v\delta f_e$, which after making use of the general equilibrium electron distribution function discussed in Section II B, yields

$$\delta\tilde{n}_e = \frac{|q|n_e\delta\tilde{E}}{mv_{Te}^2|k_y|}\int_{-\infty}^{\infty} du_\parallel \frac{i}{\zeta - u_\parallel}\frac{dG}{du_\parallel}, \tag{24}$$

where $\zeta = -\mathrm{sgn}(\mathbf{k}\cdot\mathbf{v}_{de})v_{de}/v_{Te}$. Applying the Plemelj relation to Eq. (24) above gives

$$\delta\tilde{n}_e = \frac{2|q|n_e\delta\tilde{E}}{mv_{Te}^2|k_y|}(i\alpha + \pi\beta). \tag{25}$$

Here, α and β have the same definition as that in Section II B. Then using Eq. (5) for the electron-ion friction force, and averaging over the wave period and wavelength so that $\langle\delta n_e\delta E_y\rangle = 1/2\mathrm{Re}\{\delta\tilde{n}_e\delta\tilde{E}_y^*\}$ (where the asterix denotes the complex conjugate), we find the friction force as

$$\mathbf{R}_{ei} = -\frac{\pi q^2 n_e\beta|\delta\tilde{E}_y|^2}{mv_{Te}^2|k_y|}\hat{\mathbf{j}}. \tag{26}$$

We now assume that the wavenumber, $k_y = k_{max}$, is that which occurs for the maximum growth rate, and thus Eq. (26) becomes

$$\mathbf{R}_{ei} = -\frac{\sqrt{2}\pi q^2 n_e\beta|\delta\tilde{E}_y|^2\lambda_{De}}{mv_{Te}^2}\hat{\mathbf{j}}. \tag{27}$$

The sign of the wavenumber of maximum growth rate in Eq. (19) deserves special attention. Since electrons drift upstream towards the anode in HETs, this requires $\mathbf{R}_{ei}$ to point in the negative $\hat{\mathbf{j}}$ direction (for the coordinate system used here). From Eq. (27) above, this therefore requires that

$\beta > 0$. Because $\beta = \beta(\zeta)$, and since $\zeta = -\text{sgn}(\mathbf{k}\cdot\mathbf{v}_{de})v_{de}/v_{Te}$, the direction of the azimuthal electron drift velocity determines which wavenumber to choose to ensure this.

The fact that there appears to be only a single dominant wavenumber that depends on the direction of the electron drift velocity is in excellent agreement with the experimental observations made in Ref. 42. We also note in passing that from Eq. (19), and using the numerical parameters in Section II B, we obtain an instability wavenumber and wavelength at maximum growth rate of $8500\,\text{m}^{-1}$ and 0.74 mm, respectively. These values are in very good agreement with the values of $9500\,\text{m}^{-1}$ and 0.66 mm found experimentally in Ref. 42 for a thruster operating at similar conditions. Also, for propagation in the azimuthal direction, $k_z = 0$, and from Eq. (20) the instability frequency is, $f_R = \omega_{Rmax}/2\pi \approx \pm 4.7\,\text{MHz}$. This is again in excellent agreement with the experimental value of $\pm 4.5\,\text{MHz}$.[42]

D. Ion-wave trapping

From the PIC simulations in Paper I,[31] and from the theory of beam-cyclotron instabilities,[39,45] the amplitude of an ion-acoustic instability saturates due to ion-wave trapping. Electron-wave trapping does not appear to be a feasible saturation mechanism because of the strongly enhanced electron collisionality associated with the instability. Thus, the amplitude of the potential fluctuations at saturation, $|\delta\tilde{\phi}|$, can be given by[46,47]

$$|\delta\tilde{\phi}| = \frac{1}{2}\frac{M}{q}\left(\frac{\omega_R}{k_{max}}\right)^2, \tag{28}$$

where the term in brackets is the wave phase velocity in the "azimuthal" direction. Since we have assumed sinusoidal fluctuations, $|\delta\tilde{E}| = k_{max}|\delta\tilde{\phi}|$, and using Eqs. (19) and (20) (with $k_z = 0$) we obtain

$$|\delta\tilde{E}| = \frac{1}{3\sqrt{2}}\frac{T_e}{\lambda_{De}}. \tag{29}$$

For typical plasma parameters in the thruster acceleration region (such as the numerical values in Section II B), the root-mean square electric field amplitude is $|\delta\tilde{E}|/\sqrt{2} \sim 5\times 10^4\,\text{Vm}^{-1}$. This value is similar to that seen in the PIC simulations in Refs. 13, 16, 30, and 31. The saturated amplitude from Eq. (29) is expected to be valid in the thruster acceleration region, and in the near-field downstream of the thruster exit, but not close to the anode in the upstream region. This is because the azimuthal electron drift velocity in this region is very low, and so the instability growth rate will correspondingly be smaller so that saturation might not be reached in this region.

E. Conservation of wave energy

In order to find the electron-ion friction force from Eq. (27), one needs to know β (or equivalently the electron distribution function) at saturation. This is an exceedingly challenging problem because the evolution of the distribution function is itself nonlinear. However, if the growth rate at saturation, γ^{sat}, can be determined, then the distribution function (or rather β) can be estimated directly from Eq. (16).

Since the instability wavelength is of the order of 1 mm, which is much smaller than typical spatial scales in the plasma, one can make use of ray-tracing equations to find the trajectory of the wave energy flow in the plasma.[36] Assuming that the plasma dielectric does not change on time scales similar to the instability frequency, and for a single well-defined wave packet at the wavenumber of maximum growth rate, k_{max}, the instability energy conservation equation is given by[36]

$$\frac{\partial W}{\partial t} + \nabla\cdot(\mathbf{v}_g W) = 2\gamma W, \tag{30}$$

where

$$W = \frac{1}{2}\epsilon_0|\delta\tilde{E}|^2\omega_R\left.\frac{\partial\hat{\varepsilon}}{\partial\omega}\right|_{\omega_R} \tag{31}$$

is the wave energy density. The appearance of the plasma dielectric in Eq. (31) is related to the charged particle energy associated with the instability motion.[36] From Eq. (12),

$$\frac{\partial\hat{\varepsilon}}{\partial\omega} \approx \frac{2\omega_{pi}^2}{(\omega - \mathbf{k}\cdot\mathbf{v}_{di})^3}. \tag{32}$$

Thus

$$\omega_R\left.\frac{\partial\hat{\varepsilon}}{\partial\omega}\right|_{\omega_R} \approx 6, \tag{33}$$

where we have used Eqs. (19) and (20) (with $k_z = 0$). At steady state, $\partial W/\partial t = 0$, and since the amplitude of the instability electric field is determined from the ion-wave trapping criterion found in Section II D above, Eq. 30 provides a means to determine the growth rate. Thus using Eqs. (16), (19), (22), (29), (30), (31), and (33), we have

$$\beta \approx \pm\frac{3\sqrt{3}}{2\pi}\frac{\lambda_{De}}{c_s n_e T_e}\nabla\cdot(\mathbf{v}_{di} n_e T_e). \tag{34}$$

In deriving this equation, we have used $\alpha \approx 1$ which is true for a Maxwellian distribution. Although deviations from a Maxwellian near the wave resonance significantly influence the instability through the parameter β, they have less affect on the parameter α. This is because (see Section II B) α is given by an integral over the entire velocity distribution, whereas β depends on the derivative of the distribution function near the wave resonance (see Eqs. (13) and (14)).

Recall from Section II B B that $\beta = \beta(\zeta)$ where $\zeta = (\omega - \mathbf{k}\cdot\mathbf{v}_{de})/kv_{Te} \approx -\mathbf{k}\cdot\mathbf{v}_{de}/kv_{Te}$. Since we have assumed that the instability is mainly in the azimuthal direction, this gives $\zeta \approx -\text{sgn}(\mathbf{k}\cdot\mathbf{v}_{de})v_{de}/v_{Te}$. From Section II C, we must have that $\mathbf{R}_{ei}$ is in the negative $\hat{\mathbf{j}}$ direction (which is towards the anode in the coordinate system used here), and since there are two modes in the dispersion relation, we must choose the sign of Eq. (34) to ensure this. To highlight this, we introduce an absolute value, and combine Eqs. (34) and (29) with (27) to obtain an estimate for the saturated electron-ion friction force

$$\mathbf{R}_{ei} = -\frac{q}{4\sqrt{6}}\frac{1}{c_s}|\nabla\cdot(\mathbf{v}_{di}n_eT_e)|\hat{\mathbf{j}}. \tag{35}$$

In deriving the above equation, we ignored the nonlinear terms on the right-hand side of Eq. (3), as discussed in Section II C. This is expected to be valid so long as $|\delta\tilde{n}_e|/n_e \ll 1$. From Eq. (28), we find that $|\delta\tilde{\phi}|/T_e = 1/3$, while from Eqs. (19), (25), and (29) we find that $|\delta\tilde{n}_e|/n_e = (|\delta\tilde{\phi}|/T_e)\sqrt{\alpha^2+\pi^2\beta^2} \approx |\delta\tilde{\phi}|/T_e = 1/3 < 1$. Thus ignoring the nonlinear terms in Eq. (3) is reasonably well justified.

From the 2D PIC simulations in Ref. 14, and the 1D PIC simulations in Refs. 30 and 31, the amplitude of the density fluctuations is in the range $|\delta\tilde{n}_e|/n_e \approx 0.15-0.3$, which is close to the value of 1/3 predicted with the present theory. Furthermore, in Ref. 14, for an electron temperature of 10 eV, the amplitude of the potential fluctuations was found to be about 2–4 V, which gives $|\delta\tilde{\phi}|/T_e \approx 0.2-0.4$. This again agrees well with the value of 1/3 found here.

F. Anomalous mobility/collisionality

Having obtained an expression for the electron-ion friction force, we can now determine the electron mobility and effective collision frequency. We begin by considering Eq. (2) for the electrons, but now add an additional collision operator, C_{en}, to account for electron-neutral collisions. We assume that these types of collisions have a negligible effect on the plasma dispersion relation and electron-ion friction force as calculated in the sections above (which appears justified based on the PIC simulations in Paper I[31]). Thus, Eq. (2) for electrons becomes

$$\frac{\partial f_e}{\partial t} + \mathbf{v}\cdot\frac{\partial f_e}{\partial \mathbf{x}} + \frac{q}{m}(\mathbf{E}+\mathbf{v}\times\mathbf{B})\cdot\frac{\partial f_e}{\partial \mathbf{v}} = -\frac{q}{m}\left\langle \delta\mathbf{E}\cdot\frac{\partial \delta f_e}{\partial \mathbf{v}}\right\rangle + C_{en}. \tag{36}$$

Multiplying by $m\mathbf{v}$ and integrating over all velocities, we obtain the electron momentum conservation equation

$$\frac{\partial}{\partial t}(mn_e\mathbf{v}_{de}) + \nabla\cdot(mn_e\mathbf{v}_{de}\mathbf{v}_{de}) = qn_e(\mathbf{E}+\mathbf{v}_{de}\times\mathbf{B}) - \nabla\cdot\Pi_e - m\nu_m n_e\mathbf{v}_{de} + \mathbf{R}_{ei}, \tag{37}$$

where ν_m is the electron-neutral momentum transfer collision frequency. We can then introduce an effective electron-ion collision frequency, ν_{ei}, through the definition, $\mathbf{R}_{ei} = -m\nu_{ei}n_e\mathbf{v}_{de}$. Since the electron drift is mainly in the "azimuthal" direction (and hence so to is the frictional drag), we therefore have

$$\nu_{ei} = \frac{R_{ei}}{mn_ev_{de}}, \tag{38}$$

where $R_{ei} = |\mathbf{R}_{ei}|$. By combining the momentum conservation equations in the "axial" and "azimuthal" directions (while ignoring the inertial and pressure tensor terms), we can obtain an expression for the effective mobility

$$\mu_{eff} = \frac{\frac{|q|}{m\nu_m}\left[1+\frac{\omega_{ce}}{\nu_m}\frac{R_{ei}}{|q|n_eE_z}\right]}{1+\frac{\omega_{ce}^2}{\nu_m^2}}. \tag{39}$$

This mobility is similar to that found in Paper I.[31] Finally, we make three important observations regarding Eqs. (35), (38), and (39): (1) Since the plasma parameters such as n_e, T_e, v_{di}, v_{de}, and E_z, are all, in general, implicit functions of the applied magnetic field profile and strength in the thruster, the enhanced mobility cannot, in general, be fit with simple $1/B^2$ or $1/B$ scaling laws. This conclusion agrees with that obtained experimentally in Refs. 16, 33, 34, 48, and 49. (2) Even though the electron drift velocity (and hence instability growth rate/amplitude) is largest inside the thruster, the finite wave group velocity due to ion acceleration in HETs causes a convection of the instability into the downstream region. This conclusion is also in agreement with deductions from the experiments/simulations in Ref. 50. Thus, the anomalous collisionality/mobility can be larger in this downstream region than inside the thruster itself (see Section III below). (3) Since Eq. (39) depends on the applied axial electric field itself, the concept of an electron cross-field mobility is strictly speaking no longer necessarily valid. This agrees with the conclusions drawn in Ref. 16.

III. COMPARISON WITH SIMULATION/EXPERIMENT

As seen from Eq. (35), the present theory is incomplete in the sense that we do not have a model to determine n_e, T_e, or v_{di}. These quantities need to be determined self-consistently with the new instability-enhanced theory developed here, which will require a global fluid simulation. However, previous fluid simulations[16] have made use of empirically determined electron mobilities in order to obtain agreement with experiment, and thus we can use the plasma profiles obtained from these simulations to check the kinetic theory.

Figure 2 shows the plasma profiles obtained from the simulations in Refs. 10 and 16 for the PPS®1350 thruster, while Fig. 3 shows a comparison of the empirical mobility, together with that predicted from the kinetic theory presented here and the classically expected value. Since the simulation profiles correspond to values along an axial line through the center of the thruster channel, any radial gradients vanish (i.e., $\partial/\partial r \approx 0$), and thus $\nabla\cdot(\mathbf{v}_{di}n_eT_e) \rightarrow d(v_{di}n_eT_e)/dz$ in Eq. (35). As seen, the classical mobility is close to the empirical value near the anode on the left-hand side ($z = 0$ cm) but diverges in the acceleration and downstream regions, where the classical value is 2–3 orders of magnitude smaller. In addition, the minimum mobility is predicted to occur at $z \approx 3.5$ cm, while that obtained empirically occurs at $z \approx 2.5$ cm.

In contrast, the instability-enhanced mobility is significantly larger and is of the same order of magnitude as the empirical mobility, showing particularly good agreement in the downstream region. Furthermore, the kinetic theory correctly predicts the location of the minimum mobility, which occurs when $R_{ei} = 0$. This allows us to propose a generalized

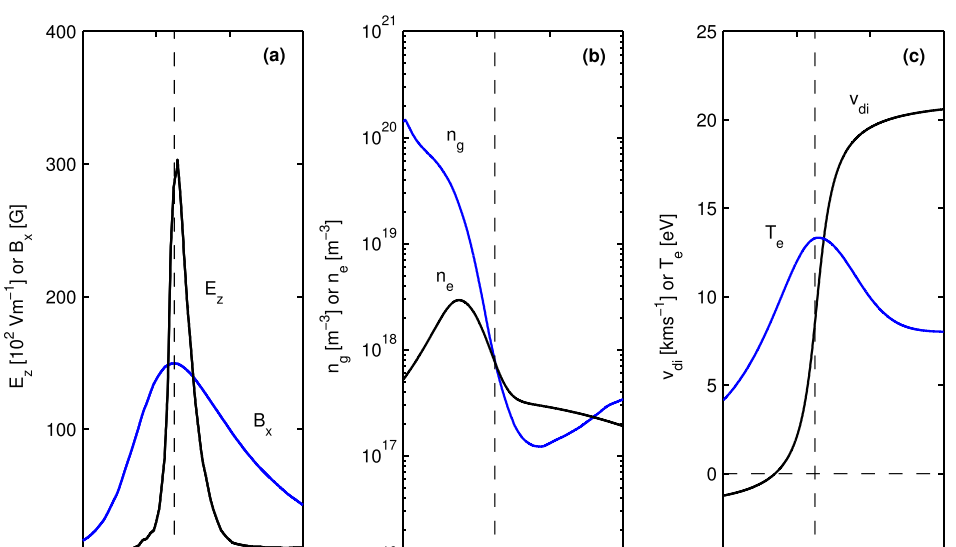

FIG. 2. (a) Axial electric field (E_z) and radial magnetic field (B_x), (b) neutral gas density (n_g) and electron density (n_e), and (c) axial ion drift velocity (v_{di}) and electron temperature (T_e), as a function of axial position within the PPS®1350 thruster. The axial profiles are taken from Refs. 10 and 16, and are along an axial line passing through the center of the thruster channel. The vertical dashed lines in (a)–(c) indicate the thruster exit plane.

criteria for finding the spatial location of this minimum mobility from

$$\frac{d}{dz}(v_{di}n_eT_e) = 0. \tag{40}$$

Inside the thruster (to the left of the vertical dashed line in Fig. 3), the kinetic theory also predicts an increased electron transport, in agreement with the empirical mobility. However, close to the anode on the left-hand side, the predicted mobility is significantly higher than the empirical values. This is expected (see Section II D), because we have assumed that the instability amplitude reaches saturation levels throughout the thruster. In this region though the electron azimuthal drift velocity is much lower, the instability growth rate is not as high and the instability is not expected to reach saturated levels in this region. In addition, the electric field taken from Ref. 16 for this calculation is close to zero near the anode (see Fig. 2(a)), which causes an unphysical overestimation of the mobility in this region. In this region though the empirical mobility is in good agreement with classical theory, so the kinetic theory is not required here. With the exception of this anode region, and given the complexity of the problem (as well as the uncertainty in the empirical mobility anyway), the kinetic theory presented here is in very good agreement with the empirical values, and represents a promising step forward.

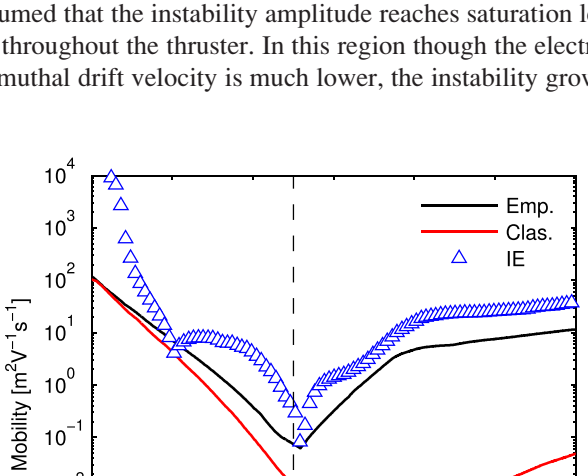

FIG. 3. Electron cross-field mobility as a function of axial position within the PPS®1350 thruster. The solid black line is an empirical mobility which is needed in fluid simulations in order to get agreement with experiment,[16] the red line is the mobility based on classical diffusion across a magnetic field, while the open blue triangles show the mobility due to the saturated instability-enhanced electron-ion friction force. The vertical dashed line indicates the thruster exit plane.

Determining the true instability amplitude at each location without assuming the saturation criterion in Section II D requires knowing how the growth rate (and hence electron distribution function) changes with time during the instability evolution. Simply assuming a growth rate given by that for a Maxwellian would result in an unphysically large mobility. This problem was recently encountered using a different model in Ref. 19. The location where $v_{di} = 0$, or $E_z = 0$, is expected to be a reasonable boundary point after which the instability amplitude reaches saturation levels. A smoother transition would be to use the point, where $\frac{d}{dz}(v_{di}n_eT_e)$ first goes to zero inside the thruster. (For the present comparison, there are two points where the derivative is zero; one inside the thruster and one outside. It is the outer point that gives the location of the minimum mobility.) Using this latter criterion and scaling the instability-enhanced mobility to fit the empirical values, we obtain the results in Fig. 4, which demonstrates the quite robust plasma parameter scaling exemplified by Eqs. (35) and (39).

IV. DISCUSSION

A. Model assumptions and limitations

As demonstrated in Section II C, the electron-cyclotron instability has a very large growth rate meaning that standard quasilinear theory is not expected to be valid. It is difficult

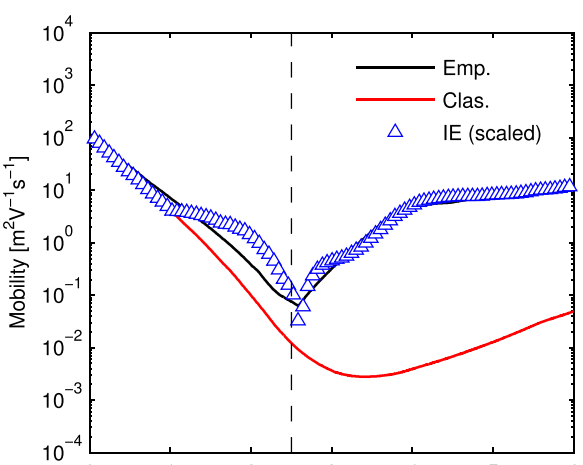

FIG. 4. Electron cross-field mobility as a function of axial position within the PPS®1350 thruster. The solid black line is an empirical mobility which is needed in fluid simulations in order to get agreement with experiment,[16] the red line is the mobility based on classical diffusion across a magnetic field, while the open blue triangles show the scaled (by a factor of about 1/3) mobility due to the saturated instability-enhanced electron-ion friction force. The instability electric field is assumed negligible to the left of the axial location where $d(v_{di}n_eT_e)/dz$ first goes to zero. The vertical dashed line indicates the thruster exit plane.

however to self-consistently include nonlinear effects while still leaving the relevant equations tractable. The nonlinear theory developed here is in some ways similar to that more rigorously developed in Ref. 51 to describe nonlinear Landau damping in that we have assumed a monochromatic instability and have tried to extend the validity of quasilinear theory by determining the saturated instability amplitude and growth rate. However, whereas saturation in Ref. 51 occurs due to electron trapping and instability convection is absent, here the cyclotron instability saturates due to ion trapping and convection is important in determining the equilibrium growth rate which does not go to zero.

To find the saturated growth rate, we made use of the dispersion relation for a modified ion-acoustic instability, and approximately accounted for nonlinear effects by using a generalized electron distribution, which would distort in a complicated (and nonlinear) manner due to velocity-space diffusion as a result of the instability. By then using the wave energy conservation equation, we were able to estimate the growth rate at saturation; without ever needing to know the exact distribution function. The basic dispersion relation though is for a uniform plasma, and still uses some elements of quasilinear theory. An improved analysis would require the more complicated nonlinear dispersion relation, such as that discussed in Ref. 52; although given the good agreement with the experimentally/numerically determined instability wavenumber/wavelength and frequency, and fluctuation amplitudes, the present analysis appears to be a good approximation. Also, we have assumed a monochromatic wave, whereas in reality a combination of frequencies and wavelengths are likely to occur to some extent. Relaxation of the above assumptions seems like a good direction for future work.

B. Secondary electron emission and rotating spokes

In the theory presented here, we have not included electron-wall collisions or secondary electron emission. This was based on the observation that previous axial-azimuthal 2D PIC simulations[13,15] did not include such effects (or demonstrated that their effect was too small) and yet still observed anomalous electron transport similar to experiments. However, it is known that changes to the thruster wall material (and hence secondary emission coefficient) have an effect on the electron transport and the thruster performance.[3,53–55] Since the electron-ion friction force (and hence mobility) found here is a strong function of the plasma density, electron temperature, ion drift velocity, magnetic field, and axial electric field inside the thruster though, it is plausible that electron emission from the channel walls plays only a secondary role. This is because electron loss and strong emission would change the electron distribution function, which is then expected to slightly change the electron temperature, plasma density (due to different ionization rates), and electric field, and changes in these quantities will consequently change the friction force/mobility. Thus, changes in the secondary electron emission coefficient will necessarily induce changes in the instability propagation and growth rate, and hence to the electron transport. The dominant and driving effect, however, is still the azimuthal instability itself.

In recent years, the study of rotating spoke phenomena and their role in cross-field electron transport has increased, with a number of experimental[27,28,56] and simulation observations.[57,58] These spokes are typically in the kHz frequency range and are associated with periodic neutral gas depletion in the azimuthal direction.[57,58] Since the kinetic theory presented here is essentially collisionless, and yet still predicts a strongly enhanced electron transport, the analysis suggests that the enhanced transport observed with rotating spokes is either due to increased electron-neutral collisionality within the spokes, or due to the formation of large-scale gradients (larger than the high-frequency instability wavelengths discussed here) in the azimuthal direction, and which would affect the dispersion relation and high-frequency instability behaviour. Such large-scale azimuthal gradients could be accounted for with the present theory by observing Eq. (35) and noting that in cylindrical coordinates, $\nabla \cdot \mathbf{A} = \partial A_z/\partial z + (1/r)\partial(rA_r)/\partial r + (1/r)\partial A_\theta/\partial\theta$, where $\mathbf{A} = \mathbf{v}_{di}n_eT_e$, and θ is the cylindrical angular coordinate.

C. Considerations for future kinetic simulations

Many 2D PIC simulations[12,15] often include a scaling factor to reduce the plasma density (or equivalently to increase the permittivity) so as to lower the computational cost of running the code. As seen from Eq. (35), the enhanced electron-ion friction force is a function of the plasma density. Hence, such PIC codes would not necessarily correctly model the instability and enhanced electron transport, and for very large scaling factors, could remove the instability altogether. This is also particularly true in PIC simulations which use a scaling factor to reduce the thruster dimensions. In this case, the convection time of the instability is artificially reduced, which again changes the instability

evolution, and in the worst case, can prevent the instability from forming (i.e., if the convection time, τ_c, is much shorter than the growth time, τ_g). The above considerations probably explain why the anomalous mobility observed in the 2D PIC simulations in Ref. 15 (where a scaling factor was used) was found to be lower than that observed in Ref. 13 (where no scaling factor was used). Furthermore, as discussed in Section II B, while the full plasma dispersion relation shows a discrete spectrum, in reality, because of the need to satisfy the wavelength matching conditions in the radial thruster direction, the actual dispersion relation is expected to be closer to the continuum spectrum of an ion-acoustic instability. Hence, 2D PIC simulations which model only the axial-azimuthal directions (and which consequently enforce $k_x = 0$) will not necessarily correctly account for the instability. This suggests that, in principle, full 3D simulations of HETs are necessary, with a grid size that sufficiently resolves the main instability wavelengths.

V. CONCLUSIONS

In summary, we have presented a kinetic model to describe the anomalous electron transport in HETs. We have shown that the dispersion relation is similar to that for an ion-acoustic wave and does not show the discrete, quantized bands observed previously, and that the maximum growth rate occurs for a wavelength of about 1 mm. In the model, the anomalous electron transport occurs because of an enhanced electron-ion frictional drag force associated with an electron cyclotron instability in the azimuthal direction due to the large azimuthal electron drift velocity. This instability grows rapidly before nonlinear effects associated with ion-wave trapping set in to limit the amplitude. The growth rate after this time does not vanish because of a nonzero group velocity, thus allowing further wave growth to be balanced by convection. This convection (due to the large ion drift velocities in the axial direction) carries the instability downstream and leads to a strong increase in the electron cross-field mobility that agrees qualitatively and quantitatively with that seen experimentally. This mobility is a strong function of almost all plasma parameters, and consequently, does not scale with simple $1/B_0^2$ or $1/B_0$ laws.

ACKNOWLEDGMENTS

The authors would like to thank Jean-Pierre Boeuf, Jean-Claude Adam, Anne Héron, Claude Boniface, Laurent Garrigues, Gerjan Hagelaar, and Stephan Zurbach for a number of useful comments and discussions. This work received financial support from a CNES postdoctoral research award.

APPENDIX: CALCULATION OF THE FULL DISPERSION RELATION

To obtain the full dispersion relation from Eqs. (6) and (7), we must first evaluate the trajectories of unperturbed particles. These trajectories are characterized by phase space coordinates given by, $\mathbf{x}'(t')$ and $\mathbf{v}'(t')$, which are found from the equations

$$\frac{d\mathbf{v}'}{dt'} = \frac{q_s(\mathbf{E} + \mathbf{v}' \times \mathbf{B})}{m_s} \quad \text{and} \quad \frac{d\mathbf{x}'}{dt'} = \mathbf{v}' \tag{A1}$$

subject to the end point conditions: $\mathbf{x}'(t' = t) = \mathbf{x}$ and $\mathbf{v}'(t' = t) = \mathbf{v}$. Also, $\tau = t - t'$ and $\mathbf{d} = \mathbf{x}' - \mathbf{x}$. By solving Eq. (A1) in the presence of constant mutually perpendicular electric and magnetic fields and applying the end point conditions, we obtain after some algebra

$$\mathbf{d} = -v_x\tau\hat{\mathbf{i}} - v_{de}\tau\hat{\mathbf{j}} + \frac{w_\perp}{\omega_{ce}}[\sin\phi - \sin(\phi + \omega_{ce}\tau)]\hat{\mathbf{j}} + \frac{w_\perp}{\omega_{ce}}[\cos(\phi + \omega_{ce}\tau) - \cos\phi]\hat{\mathbf{k}}, \tag{A2}$$

where $w_\perp^2 = v_z^2 + (v_y - v_{de})^2$ and $\tan\phi = v_z/(v_y - v_{de})$. By then defining $k_\perp^2 = k_y^2 + k_z^2$ and $\tan\psi = k_z/k_y$, substituting Eq. (A2) into Eq. (7), and using standard trigonometric identities together with the Jacobi-Auger relations, Eq. (7) becomes

$$\frac{1}{\bar{\omega}_p} = \sum_n \sum_m \frac{J_n(\beta)J_m(\beta)e^{i(\phi-\psi)(n-m)}}{\omega - k_x v_x - k_y v_{de} - m\omega_{ce}}. \tag{A3}$$

Here, J_n are Bessel functions of the first kind, $\beta = k_\perp^2 v_{Te}^2/2\omega_{ce}$, $v_{Te} = \sqrt{2qT_e/m}$, and n and m are summation indices. Substituting this into Eq. (6), assuming drifting Maxwellian distributions for both electrons and ions, and making use of the Bessel function identities on page 253 of Ref. 36, together with the identity, $\sum_{n=-\infty}^{\infty} e^{-\beta} I_n(\beta) = 1$, the integrals can be performed providing

$$\hat{\varepsilon}(\mathbf{k},\omega) = 1 - \frac{\omega_{pi}^2}{k^2 v_{Ti}^2} Z'\left(\frac{\omega - \mathbf{k}\cdot\mathbf{v}_{di}}{k v_{Ti}}\right) + \frac{1}{k^2\lambda_{De}^2}\left[1 + \left(\frac{\omega - k_y v_{de}}{k v_{Te}}\right)\sum_{n=-\infty}^{\infty} e^{-\beta} I_n(\beta) Z \times \left(\frac{\omega - k_y v_{de} - n\omega_{ce}}{k_x v_{Te}}\right)\right], \tag{A4}$$

where I_n are modified Bessel functions of the first kind. This is identical to the dispersion relation first presented in Ref. 32, except that we have included an ion drift velocity. By setting $\hat{\varepsilon}(\mathbf{k},\omega) = 0$, we obtain the dispersion relation. This relation can be solved numerically by making use of the Gordeev function and the iterative scheme proposed in Ref. 40. If we go back to Eq. (A2), we observe that $\omega_{ce}\tau \sim \omega_{ce}/kw_\perp = 1/k\rho$, where ρ is the electron gyroradius. Since the instability wavelengths of interest are of the order of the Debye length, we have $k \sim 1/\lambda_{De}$, and thus $\omega_{ce}\tau \sim \lambda_{De}/\rho$. However, in typical HETs we have $\lambda_{De}/\rho \ll 1$. Thus, we can expand the sin and cos functions in Eq. (A2) to first order to obtain

$$\mathbf{d} = -v_x\tau\hat{\mathbf{i}} - v_y\tau\hat{\mathbf{j}} - v_z\tau\hat{\mathbf{k}}. \tag{A5}$$

In this case, Eq. (7) simplifies to

$$\frac{1}{\bar{\omega}_p} = \frac{1}{\omega - \mathbf{k}\cdot\mathbf{v}}. \tag{A6}$$

This form for $\bar{\omega}_p$ is used in the derivation of the modified ion-acoustic dispersion relation in Section II B.

[1]V. V. Zhurin, H. R. Kaufman, and R. S. Robinson, Plasma Sources Sci. Technol. **8**, R1 (1999).
[2]A. I. Morozov and V. V. Savelyev in *Reviews of Plasma Physics*, edited by B. B. Kadomtsev and V. D. Shafranov (Springer Science+Business Media, New York, 2000).
[3]D. M. Goebel and I. Katz, *Fundamentals of Electric Propulsion: Ion and Hall Thrusters*(Wiley, New Jersey, 2008).
[4]S. Samukawa *et al*., J. Phys. D: Appl. Phys. **45**, 253001 (2012).
[5]S. Mazouffre, F. Dubois, L. Albaréde, D. Pagnon, M. Touzeau, and M. Dudeck, *Proceedings of the International Conference on Recent Advances in Space Technologies (RAST'03)* (IEEE, 2003), pp. 69–74.
[6]I. G. Mikellides and I. Katz, Phys. Rev. E **86**, 046703 (2012).
[7]S. Barral and E. Ahedo, Phys. Rev. E **79**, 046401 (2009).
[8]M. Keidar, I. D. Boyd, and I. I. Beilis, Phys. Plasmas **8**, 5315 (2001).
[9]J. P. Boeuf and L. Garrigues, J. Appl. Phys. **84**, 3541 (1998).
[10]J. Bareilles, G. J. M. Hagelaar, L. Garrigues, C. Boniface, J. P. Boeuf, and N. Gascon, Phys. Plasmas **11**, 3035 (2004).
[11]C. M. Lam, A. K. Knoll, M. A. Cappelli, and E. Fernandez, in *31st International Electric Propulsion Conference* (The Electric Rocket Propulsion Society, Ann Arbor, MI, 2009), paper no. IEPC-2009-102.
[12]J. J. Sazbo, "Fully kinetic modeling of a plasma thruster," Ph.D. thesis, Massachusetts Institute of Technology, 2001.
[13]J. C. Adam, A. Héron, and G. Laval, Phys. Plasmas **11**, 295 (2004).
[14]A. Héron and J. C. Adam, Phys. Plasmas **20**, 082313 (2013).
[15]P. Coche and L. Garrigues, Phys. Plasmas **21**, 023503 (2014).
[16]J. C. Adam, J. P. Boeuf, N. Dubuit, M. Dudeck, L. Garrigues, D. Gresillon, A. Heron, G. J. M. Hagelaar, V. Kulaev, N. Lemoine, S. Mazouffre, J. Perez Luna, V. Pisarev, and S. Tsikata, Plasma Phys. Controlled Fusion **50**, 124041 (2008).
[17]G. J. M. Hagelaar, J. Bareilles, L. Garrigues, and J. P. Boeuf, J. Appl. Phys. **93**, 67 (2003).
[18]J. W. Koo and I. D. Boyd, Phys. Plasmas **13**, 033501 (2006).
[19]I. Katz, I. G. Mikellides, B. A. Jorns, and A. L. Ortega, in *Joint Conference of 30th International Symposium on Space Technology and Science 34th International Electric Propulsion Conference and 6th Nano-satellite Symposium* (The Electric Rocket Propulsion Society, Hyogo-Kobe, Japan, 2015), paper no. IEPC-2015-402.
[20]F. I. Parra, E. Ahedo, J. M. Fife, and M. Martínez-Sánchez, J. Appl. Phys. **100**, 023304 (2006).
[21]M. K. Scharfe, N. Gascon, M. A. Cappelli, and E. Fernandez, Phys. Plasmas **13**, 083505 (2006).
[22]A. N. Smirnov, Y. Raitses, and N. J. Fisch, IEEE Trans. Plasma Sci. **34**, 132 (2006).
[23]E. Y. Choueiri, Phys. Plasmas **8**, 1411 (2001).
[24]G. S. Janes and R. S. Lowder, Phys. Fluids **9**, 1115 (1966).
[25]A. W. Smith and M. A. Cappelli, Phys. Plasmas **16**, 073504 (2009).
[26]S. Yoshikawa and D. J. Rose, Phys. Fluids **5**, 334 (1962).
[27]J. B. Parker, Y. Raitses, and N. J. Fisch, Appl. Phys. Lett. **97**, 091501 (2010).
[28]C. L. Ellison, Y. Raitses, and N. J. Fisch, Phys. Plasmas **19**, 013503 (2012).
[29]M. Hirakawa, in *25th International Electric Propulsion Conference* (The Electric Rocket Propulsion Society, Worthington, OH, 1997), paper no. IEPC-97-021.
[30]J. P. Boeuf, Front. Phys. **2**, 74 (2014).
[31]T. Lafleur, S. D. Baalrud, and P. Chabert, "Theory for the anomalous electron transport in Hall effect thrusters. I. Insights from particle-in-cell simulations," Phys. Plasmas **23**, 053502 (2016).
[32]A. Ducrocq, J. C. Adam, A. Héron, and G. Laval, Phys. Plasmas **13**, 102111 (2006).
[33]L. Garrigues, J. Pérez-Luna, J. Lo, G. J. M. Hagelaar, J. P. Boeuf, and S. Mazouffre, Appl. Phys. Lett. **95**, 141501 (2009).
[34]R. R. Hofer, I. Katz, I. G. Mikellides, D. M. Goebel, K. K. Jameson, R. M. Sullivan, and L. K. Johnson, in *44th AIAA/ASME/SAE/ASEE Joint Propulsion Conference and Exhibit* (American Institute of Aeronautics and Astronautics, Hartford, CT, 2008), paper no. AIAA-2008-4924.
[35]M. A. Cappelli, C. V. Young, E. Cha, and E. Fernandez, Phys. Plasmas **22**, 114505 (2015).
[36]T. H. Stix, *Waves in Plasmas* (Springer-Verlag, New York, 1992).
[37]S. D. Baalrud, "Kinetic theory of instability-enhanced collective interactions in plasma," Ph.D. thesis, University of Wisconsin-Madison, 2010.
[38]S. D. Baalrud, J. D. Callen, and C. C. Hegna, Phys. Plasmas **15**, 092111 (2008).
[39]M. Lampe, W. M. Manheimer, J. B. McBride, J. H. Orens, K. Papadopoulos, R. Shanny, and R. N. Sudan, Phys. Fluids **15**, 662 (1972).
[40]J. Cavalier, N. Lemoine, G. Bonhomme, S. Tsikata, C. Honoré, and D. Grésillon, Phys. Plasmas **20**, 082107 (2013).
[41]B. D. Fried and S. D. Conte, *The Plasma Dispersion Function* (Academic Press, New York, 1961).
[42]S. Tsikata, N. Lemoine, V. Pisarev, and D. M. Grésillon, Phys. Plasmas **16**, 033506 (2009).
[43]A. Lazurenko, G. Coduti, S. Mazouffre, and G. Bonhomme, Phys. Plasmas **15**, 034502 (2008).
[44]R. C. Davidson, *Methods in Nonlinear Plasma Theory* (Academic Press, New York, 1972).
[45]M. Lampe, W. M. Manheimer, J. B. McBride, J. H. Orens, R. Shanny, and R. N. Sudan, Phys. Rev. Lett. **26**, 1221 (1971).
[46]R. L. Dewar, Phys. Fluids **16**, 431 (1973).
[47]K. Nishikawa and C. S. Wu, Phys. Rev. Lett. **23**, 1020 (1969).
[48]I. G. Mikellides, I. Katz, and R. R. Hofer, *47th AIAA/ASME/SAE/ASEE Joint Propulsion Conference and Exhibit* (American Institute of Aeronautics and Astronautics, San Diego, CA, 2011), paper no. AIAA-2011-5809.
[49]A. L. Ortega and I. G. Mikellides, *Joint Conference of 30th International Symposium on Space Technology and Science 34th International Electric Propulsion Conference and 6th Nano-satellite Symposium* (The Electric Rocket Propulsion Society, Hyogo-Kobe, Japan, 2015), paper no. IEPC-2015-310.
[50]C. Honoré, S. Tsikata, D. Grésillon, A. Héron, J. Cavalier, and N. Lemoine, *32nd International Electric Propulsion Conference* (The Electric Rocket Propulsion Society, Wiesbaden, Germany, 2011), paper no. IEPC-2011-208.
[51]T. O'Neil, Phys. Fluids **8**, 2255 (1965).
[52]A. M. Sleeper, J. Weinstock, and B. Bezzerides, Phys. Fluids **16**, 1508 (1973).
[53]N. Gascon, M. Dudeck, and S. Barral, Phys. Plasmas **10**, 4123 (2003).
[54]I. D. Kaganovich, Y. Raitses, D. Sydorenko, and A. Smolyakov, Phys. Plasmas **14**, 057104 (2007).
[55]D. Sydorenko, A. Smolyakov, I. Kaganovich, and Y. Raitses, Phys. Plasmas **15**, 053506 (2008).
[56]M. S. McDonald, "Electron transport in Hall thrusters," Ph.D. thesis, University of Michigan, 2012.
[57]K. Matyash, R. Schneider, S. Mazouffre, S. Tsikata, Y. Raitses, and A. Diallo, *33rd International Electric Propulsion Conference* (The Electric Rocket Propulsion Society, Washington, DC, 2013), paper no. IEPC-2013-307.
[58]K. Matyash, R. Schneider, O. Kalentev, Y. Raitses, and N. J. Fisch, *32nd International Electric Propulsion Conference* (The Electric Rocket Propulsion Society, Wiesbaden, Germany, 2011), paper no. IEPC-2011-070.